





Cornerstone: Octree Construction Algorithms for Scalable Particle Simulations

Sebastian Keller 
 sebastian.keller@cscs.ch
 Swiss National Supercomputing
 Center (CSCS), Switzerland

Aurélien Cavelan 
 aurelien.cavelan@unibas.ch
 University of Basel, Switzerland

Rubén Cabezon 
 ruben.cabezon@unibas.ch
 University of Basel, Switzerland




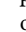
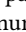
Lucio Mayer 
 lmayer@physik.uzh.ch
 University of Zürich, Switzerland

Florina M. Ciorba 
 florina.ciorba@unibas.ch
 University of Basel, Switzerland

ABSTRACT

This paper presents an octree construction method, called Cornerstone, that facilitates global domain decomposition and interactions between particles in mesh-free numerical simulations. Our method is based on algorithms developed for 3D computer graphics, which we extend to distributed high performance computing (HPC) systems. Cornerstone yields global and locally essential octrees and is able to operate on all levels of tree hierarchies in parallel. The resulting octrees are suitable for supporting the computation of various kinds of short and long range interactions in N-body methods, such as Barnes-Hut and the Fast Multipole Method (FMM). While we provide a CPU implementation, Cornerstone may run entirely on GPUs. This results in significantly faster tree construction compared to execution on CPUs and serves as a powerful building block for the design of simulation codes that move beyond an offloading approach, where only numerically intensive tasks are dispatched to GPUs. With data residing exclusively in GPU memory, Cornerstone eliminates data movements between CPUs and GPUs. As an example, we employ Cornerstone to generate locally essential octrees for a Barnes-Hut treecode running on almost the full LUMI-G system with up to 8 trillion particles.

ACM Reference Format:

Sebastian Keller , Aurélien Cavelan , Rubén Cabezon , Lucio Mayer , and Florina M. Ciorba . 2023. Cornerstone: Octree Construction Algorithms for Scalable Particle Simulations. In *Platform for Advanced Scientific Computing Conference (PASC '23)*, June 26–28, 2023, Davos, Switzerland. ACM, New York, NY, USA, 10 pages. <https://doi.org/10.1145/3592979.3593417>

1 INTRODUCTION

Octrees serve a variety of purposes in particle-based simulations. With applications in Astrophysics and Cosmology [12, 20, 23], Smoothed Particle Hydrodynamics (SPH) [9, 16], and Molecular Dynamics [21], they are typically employed to decompose domains, identify halo particle regions, solve the neighbor-search problem,

calculate global magnitudes efficiently [19], and support the analysis of simulation data [15]. If long-range interactions are involved, as is the case in electrostatics or gravity, octrees also form the basis for algorithms like Barnes-Hut [2] and the Fast Multipole Method (FMM) [10]. With ever increasing compute power ratios between GPUs and CPUs, the need to also perform tree construction and traversal on the GPU is increasing, despite the usually lower numerical intensity compared to the particle force calculations. With seemingly sequential dependencies between tree levels and memory layout concerns, efficient octree construction and traversal on GPUs remain a difficult problem.

Nevertheless, there has been a lot of progress in recent years in the field of 3D computer graphics where octrees form the first step in the construction of bounding volume hierarchies for collision detection. Several octree construction algorithms [1, 14] operate in parallel on all levels of the tree hierarchy and store data compactly in linear buffers. As a first step, these algorithms rely on the computation of sorted Morton codes [17] for the 3D objects present in the scene, which are then treated as the leaves of a binary radix tree. Hence, if we were to apply these algorithms directly to the particles in a numerical simulation, the resulting binary radix tree would resolve every particle in a separate leaf node. When calculating physical particle-particle interactions, however, we have the option of reducing the number of tree nodes and allowing multiple particles per leaf node. With increasing number of particles per leaf, the overhead due to processing tree nodes decreases while the overhead due to decreasing search efficiency for neighbor particles increases. These two opposite trends lead to an optimum balance that must be determined empirically by varying the maximum number of particles permitted per leaf node; this is commonly referred to as N_{crit} [3].

In this work, we present a new octree construction method that combines the favorable property of operating on all levels of the tree in parallel on GPUs with the option of choosing $N_{crit} > 1$. Starting from the aforementioned methods developed for 3D computer graphics, we achieve this by aggregating the space filling curve (SFC) [18] keys of particles, into a histogram before generating the internal tree nodes. The placement and size of the histogram bins are themselves defined by SFC keys and are subject to certain constraints that cause each bin to correspond to a leaf node of an octree. All bins together cover the entire SFC, and thus each SFC key in the histogram delimits the start and end of an octree leaf node, which is why we call this histogram cornerstone array. Our

Permission to make digital or hard copies of all or part of this work for personal or classroom use is granted without fee provided that copies are not made or distributed for profit or commercial advantage and that copies bear this notice and the full citation on the first page. Copyrights for components of this work owned by others than the author(s) must be honored. Abstracting with credit is permitted. To copy otherwise, or republish, to post on servers or to redistribute to lists, requires prior specific permission and/or a fee. Request permissions from permissions@acm.org.
 PASC '23, June 26–28, 2023, Davos, Switzerland

© 2023 Copyright held by the owner/author(s). Publication rights licensed to ACM.
 ACM ISBN 979-8-4007-0190-0/23/06...\$15.00
<https://doi.org/10.1145/3592979.3593417>

method works for the Morton Z-curve as well as a 3D version of the Hilbert curve [11, 13]. We employ the latter in our simulations due to its superior locality preserving properties compared to the Morton Z-curve.

We then apply the cornerstone array to the computation of locally essential trees (LET) [24] in the context of distributed numerical particle simulations. A novel feature of our LET implementation is that the determination of LET branches to be exchanged with remote subdomains is carried out on GPUs, as is the subsequent communication.

Finally, as a proof of concept, we present a Barnes-Hut treecode implementation that traverses the LET generated by our method. It is performance-portable between AMD and NVIDIA GPUs and able to scale to trillions of particles.

In the following, Sec. 3 introduces relevant properties of SFCs and their connections to octrees. Sec. 4 describes our iterative method for generating octree leaf nodes with particle counts bounded by N_{crit} , while Sec. 5 illustrates how the internal part of the octree can be computed. The extension to distributed octrees is discussed in Secs. 6 and 7 before we discuss results and future work in Sec. 8.

2 RELATED WORK

In the context of N-body simulations, Burtscher and Pingali [8], shortly followed by Bédorf et al., [5] were the first to generate octrees on GPUs as the basis for Barnes-Hut treecodes. In both approaches, the octree was constructed level by level on a single GPU. Bédorf et al. later extended their method [4] to distributed HPC systems with GPU accelerators and combined SFC-based domain decomposition with the LET method, handling the non-local parts of generating the LET on the CPU.

With the aim of improving the speed of bounding volume hierarchy generation for applications in 3D computer graphics, Karras [14] was the first to present an algorithm for binary radix tree construction that generated all levels of the tree in parallel and used it as a building block to generate octrees as well. Apetrei [1] further refined the algorithm by replacing binary searches with atomic operations. A shared trait between both approaches is that the resulting binary radix or octrees resolve each 3D object in a separate leaf cell.

3 SPACE FILLING CURVES AND OCTREES

Space filling curves (SFCs) are continuous functions that map the unit interval into an n -dimensional hypercube. In conjunction with three-dimensional particle simulations, we are interested in discretized versions of SFCs that map the key space $[0 \dots 2^{3L})$ onto a grid of 3D integer coordinates $[0 \dots 2^L) \times [0 \dots 2^L) \times [0 \dots 2^L)$. In 3D, the number of bits required to store an SFC key or a point on the grid equals $3L$. Since current computer architectures have instructions for either 32- or 64-bit integers, reasonable choices for L are 10 or 21, or – depending on accuracy requirements – multiples thereof.

The utility of certain SFCs for numerical simulations stems from their relation to octrees. If we express a key k of the Morton Z-curve with $3L$ bits as a sequence of L octal digits,

$$k = k_1 k_2 \dots k_L, \quad (1)$$

Warren and Salmon found [23] that if the first octal digit l_1 of another key l matches k_1 , then k and l decode into 3D coordinates that lie in the same octant of the root octree node. And by induction: if the first i octal digits of keys k and l match, then there exists an octree node at the i -th division level that contains the decoded 3D coordinates of both keys. Equivalently, an octree node at the i -th division level contains the 3D coordinates that encode into the key range $[k \dots k + 8^{L-i})$ for some unique k with $k \bmod 8^{L-i} = 0$. Consequently, the number of octal digits L in the SFC key is equal to the octree depth that the key is able to resolve. More generally, this correspondence between octal digits of the key and nodes of an octree applies to any type of SFC that traverses a cube octant by octant, with the Hilbert curve as a further example. The encoding and decoding of 3D grid points into Hilbert keys is computationally expensive compared to the simpler Morton Z-curve, but in contrast to the latter, any continuous segment of the curve is mapped to a compact 3D volume, while an interval of Morton keys may correspond to disconnected 3D volumes. In distributed simulations, the smaller surfaces of subdomains defined as segments of the Hilbert curve require less communication, outweighing the higher computational cost of key encoding compared to the Morton Z-curve [4].

4 LEAF NODES OF BALANCED OCTREES

As described in the previous section, arrays of space filling curve (SFC) keys can be used to represent the leaves of arbitrary octrees. Let \mathbf{K} be an array of SFC keys of length $n_l + 1$ subject to the following constraints:

$$\begin{aligned} \mathbf{K}_0 &= 0, \\ \mathbf{K}_{n_l} &= 8^L, \\ \mathbf{K}_i &< \mathbf{K}_j, \quad i < j, \quad \text{and} \\ \mathbf{K}_{i+1} - \mathbf{K}_i &= \delta_i = 8^l, \quad l \in \mathbb{N}_0, \quad l \leq L. \end{aligned} \quad (2)$$

Then, \mathbf{K} , which we refer to as the cornerstone array, uniquely defines an octree with n_l leaves and a maximum depth of L . In this notation and ordering, the i -th leaf covers the key range $[\mathbf{K}_i, \mathbf{K}_{i+1})$ and its division level is $L - \log_8 \delta_i$. Given an ensemble of real-valued 3D particle coordinates, we want to calculate \mathbf{K} , such that the leaf particle counts remain below a predefined threshold, i.e. $N_l \leq N_{\text{crit}}$, while the particle counts of internal nodes exceed N_{crit} . If these conditions are satisfied, we say that \mathbf{K} is balanced, which is a requirement for efficient particle neighbor searches. Note that since here the term *balanced* refers to a property of the leaf nodes (the number of contained particles) rather than to a property of the tree itself, its depth can vary locally. The variable N_{crit} is a performance tuning parameter in this context whose optimal value has to be determined empirically. Commonly, N_{crit} is chosen in the range 16 to 64 [3, 4, 25].

Let \mathbf{P} be the sorted array of particle SFC keys obtained by encoding the particle coordinates into SFC keys followed by a radix-sort. We define two operations:

$$f : (\mathbf{P}, \mathbf{K}) \mapsto \mathbf{N} \quad (\text{keys histogram}) \quad (3)$$

$$g : (\mathbf{K}, \mathbf{N}) \mapsto \mathbf{K}' \quad (\text{rebalancing}) \quad (4)$$

The f operation counts the number of particle keys in each leaf node, or in other words, \mathbf{N} is the histogram of particle SFC keys

\mathbf{P} for the n_i bins defined by consecutive keys in \mathbf{K} . With \mathbf{P} sorted, the particle count of the i -th bin delimited by \mathbf{K}_i and \mathbf{K}_{i+1} can be determined by locating \mathbf{K}_i and \mathbf{K}_{i+1} in \mathbf{P} with binary searches. The particle count of the bin is then given by the difference of the two delimiter positions. The g operation rebalances a given cornerstone array based on particle counts where each leaf node can either remain unchanged, be subdivided or be merged. The merging of leaf nodes is achieved by replacing a group of 8 sibling nodes with their common parent node.

We further subdivide $g = g_3 \circ g_2 \circ g_1$ into three steps:

$$g_1 : (\mathbf{K}, \mathbf{N}) \mapsto \mathbf{O}, \quad (\text{rebalancing decision}) \quad (5)$$

$$g_2 : \mathbf{O} \mapsto \mathbf{O}' \quad (\text{exclusive prefix sum}) \quad (6)$$

$$g_3 : (\mathbf{K}, \mathbf{O}') \mapsto \mathbf{K}' \quad (\text{node rebalancing}) \quad (7)$$

First, g_1 computes an auxiliary array \mathbf{O} that encodes the rebalance operation that is to be performed on each leaf node, which can be either removal, subdivision, or no change of the leaf node. These sub-operations are encoded as follows:

- $\mathbf{O}_i = 8$ if $N_i > N_{\text{crit}}$, indicating that leaf \mathbf{K}_i is to be subdivided.
- $\mathbf{O}_i = 0$ if
 - \mathbf{K}_i is not the first octant.
 - \mathbf{K}_i and its other 7 sibling octants are next to each other, i.e. when

$$\mathbf{K}_{i-j} + 8\delta_i = \mathbf{K}_{i-j+8},$$

with $j = \frac{\mathbf{K}_i \bmod 8\delta_i}{\delta_i} \in [0 \dots 7]$. This is only possible if all 8 octants are leaves.

- The combined particle count of these 8 octants is smaller than N_{crit} .

If all three conditions are fulfilled \mathbf{K}_i will not be transferred to \mathbf{K}' , resulting in the replacement of a group of 8 sibling nodes with their parent node.

- $\mathbf{O}_i = 1$ otherwise, leaving the leaf node unchanged.

Subsequently, \mathbf{O}' is obtained through g_2 by performing an exclusive prefix sum on \mathbf{O} . By construction, \mathbf{O}'_i is equal to the index of the old node \mathbf{K}_i in the rebalanced node array \mathbf{K}' , and \mathbf{O}'_{n_i} is equal to the total number of rebalanced leaf nodes in \mathbf{K}' . The rebalance step g_3 therefore constructs \mathbf{K}' as follows:

$$\mathbf{K}'_{\mathbf{O}'_i} = \mathbf{K}_i \quad \text{if } \mathbf{O}_i = 1, \quad (8)$$

$$\mathbf{K}'_{\mathbf{O}'_i+j} = \mathbf{K}_i + j \cdot \delta_i/8, j = [0 \dots 7] \quad \text{if } \mathbf{O}_i = 8. \quad (9)$$

In Eq. (8), the SFC key at \mathbf{K}_i is copied to its new location \mathbf{O}'_i in the rebalanced array \mathbf{K}' while in Eq. (9), \mathbf{K}_i is subdivided by inserting into \mathbf{K}' the 8 SFC keys of its child nodes that divide the original key range $[\mathbf{K}_i \dots \mathbf{K}_{i+1})$ into 8 sub-ranges of equal length. Fig. 1 shows an example where one of the octants of the root node is further subdivided by inserting the SFC keys of its children into the cornerstone array.

By applying f and g in alternating fashion, we can construct the leaf nodes of a balanced octree, i.e. one whose leaf node particle counts remain below or equal to N_{crit} , while the particle counts of internal nodes are greater than N_{crit} . Starting with the root node, $\mathbf{K} = \{0, 8^L\}$, alternating application of f and g then yields the balanced cornerstone array \mathbf{K}' . We say that convergence is reached when $\mathbf{O}_i = 1, \forall i$, i.e. when g_1 reports that no leaf nodes need to

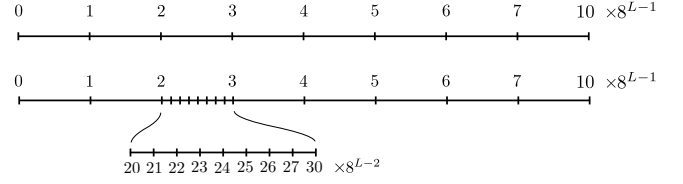


Figure 1: Example of a cornerstone array undergoing refinement. The third octant in the top panel is replaced by its 8 child nodes, resulting in an array that corresponds to the octree shown in Fig. 2. SFC keys are labeled in octal representation.

be merged or subdivided anymore, which will take at most L repeated invocations of f and g . When computing a cornerstone array by starting from just the root node, our method thus offers no advantage over a conventional top-down level-sequential octree construction approach. The utility of our method arises when octrees are built repeatedly for multiple steps with particle positions only changing by a small amount between each step. This applies, for example, to particle simulations that are performed for several time-steps. In this situation, we can maintain a cornerstone array balanced by performing a single histogram count and rebalance update on the cornerstone array of the previous step. Implicitly, \mathbf{K} contains the size and location of internal octree nodes as well, but traversal and storing additional node properties is not possible in a straightforward manner. We describe the explicit construction of internal nodes in section 5.

In terms of computational building blocks, the construction of cornerstone arrays relies on radix sort for the particle SFC keys and on and prefix sums for rebalancing, which are available from parallel libraries for both CPU and GPU architectures, such as the Thrust library [6]. The remaining operations, SFC key generation from 3D particle coordinates, f , g_1 , and g_3 consist of purely independent operations on array elements. Since there is no need for synchronization or communication, these operations are simple to implement in parallel with directive-based (e.g., OpenMP, OpenACC) as well as accelerator-specific programming paradigms (e.g., CUDA, HIP).

5 FULLY LINKED OCTREES

Although cornerstone arrays implicitly contain the information of the full octree, they are not traversable because parent-child node relationships are not stored. To efficiently generate the missing internal nodes, we will adapt the algorithms by Karras [14] and Apetrei [1]. Both originate in the computer graphics community and may be used for 3D collision detection via the generation of bounding volume hierarchies, or for ray tracing.

Either approach relies on the computation of sorted SFC keys for the objects present in a 3D scene as a first step. Subsequently, the SFC keys of the objects are viewed as the leaves of a binary radix tree whose internal nodes can be generated in parallel. A sequence of N sorted object SFC keys leads to a hierarchy of $N - 1$ internal

binary radix nodes. Each binary radix node is associated with a key that corresponds to the bit-string of the longest common prefix of all the keys that it covers, i.e. the root node has a key of length 0, and its two children have keys of length 1 consisting of either a 0 or a 1-bit. While the ordering of the $N - 1$ binary radix nodes differs between the two approaches of Karras and Apetrei, either method defines a specific node layout that allows the determination of the node bit-string keys as well as parent-child relationships of the $N - 1$ internal binary radix nodes in a data-parallel fashion. The resulting binary tree is compact in the sense that it does not contain any empty nodes or nodes with only a single child, which is a favorable property when $N_{\text{crit}} = 1$. As Karras mentions, it can be converted to an octree by extracting the binary nodes whose key lengths are divisible by 3. In practice, this conversion may be implemented in the same spirit as Eqs. (5) - (7): First, for each binary node, a value of 0 or 1 is stored in the O array depending on whether the node key length is divisible by 3 or not. After a prefix sum of O , the total number of octree nodes is then known and the relevant binary nodes may be extracted in parallel.

Since the cornerstone arrays contain SFC keys as well, we may provide them instead of the particle SFC keys as inputs to the binary radix tree construction. This allows us to take advantage of the fully parallel construction of internal nodes as well as adjusting N_{crit} to our needs (constructing the binary radix tree from the particle SFC keys would yield a tree with $N_{\text{crit}} = 1$). If we wanted to preserve the compactness property, we could now eliminate any empty buckets from K and construct the internal part of the octree as described above. But as we're interested in the case $N_{\text{crit}} > 1$, we are going to explore a second option where we do not eliminate any empty buckets from K , which is equivalent to mandating that each internal octree node have exactly 8 children. In this case, we can derive an analytical mapping between the keys in K and the internal octree nodes that they implicitly contain that allows us to bypass the construction of an intermediate binary radix tree. The resulting octree will contain a small fraction of empty nodes, depending on the value of N_{crit} and the distribution of particles, but for $N_{\text{crit}} = 16 - 64$ we have found that the increase in construction speed outweighs the penalty of a slightly larger tree, even for highly clustered distributions.

The data format for the complete octree consists of the following arrays of integer types:

- (1) $NK[n]$ in $[0, 2^{3L})$, the node SFC keys
- (2) $CO[n]$ in $[1, n)$, the connectivity array
- (3) $LO[L + 2]$ in $[1, n)$, the tree level offsets

where $n = n_i + n_l$ is the total number of tree nodes, with n_i as the number of internal nodes and n_l as the number of leaves. Since the number of children per node is either 0 or 8, $n_i = (n_l - 1)/7$. In brackets for each array, we first specify its length, followed by the range of values that its elements may assume. The first array contains the SFC keys of each node in the placeholder bit format defined in Ref. [23], which allows encoding the SFC range covered by the node with a single key. As the SFC keys can be decoded into 3D coordinates, NK stores the 3D grid coordinates of each node. The connectivity of the tree is contained in CO which stores the index of the first child. The range of child indices of node i is therefore given by $[CO[i], CO[i] + 8)$. If $CO[i] = 0$, index i corresponds to a

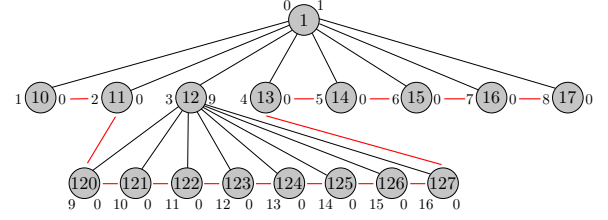


Figure 2: A linked octree with node SFC keys in placeholder-bit format contained in the gray circles. The number to the left and right of the circles show the node indices and child node indices, respectively. The red line connects the leaf nodes whose keys appear in the corresponding cornerstone array depicted in the lower panel of Fig. 1.

leaf. Lastly, the i -th element of LO contains the index of the first node at the i -th octree level where L is the maximum octree depth that the keys contained in NK are able to encode. Since we include the root node at level zero, $L + 1$ entries are required to store the offset of each level plus an additional element to mark the end of the last level. In Fig. 2 we illustrate this format with an example. The gray circles correspond to the nodes and contain the SFC keys from NK , each of which start with a 1-digit (the placeholder bit) followed by l octal digits where l is the tree level of the node. The numbers to the left of the circles indicate the node indices and the numbers to the right show the values of the CO array. For this example, the tree level offsets are $LO = \{0, 1, 9, 17, \dots, 17\}$.

To generate octrees in this format, we perform the following steps:

- (1) Copy K to $NK[n_i, n]$ and convert to the Warren-Salmon placeholder-bit format
- (2) Generate internal node keys $NK[0, n_i]$: For elements of K in parallel compute $d = \text{clz}(K[i] \wedge K[i+1])$, where clz counts the number of leading zero bits. If $\text{mod}(d, 3) = 0$, K_i is the key of an internal node at level $d/3$. The corresponding placeholder-bit key is stored at NK_j with $j = (i - \delta(K_i, d))/7$, where δ is defined below. This step can be combined with step 1.
- (3) Radix sort NK to yield a breadth-first node ordering.
- (4) Determine LO with a binary-search over NK .
- (5) Locate the first child of internal nodes with a binary-search, using LO to narrow the search range and store in CO .

The δ function that maps indices of leaf nodes to indices of internal nodes is given by

$$\delta(K_i, d) = \sum_l^{\lfloor d/3+1 \rfloor} \mu_{k_l}, \quad \mu_0, \dots, \mu_7 = \{0, -1, -2, -3, 3, 2, 1, 0\}, \quad (10)$$

where $K_i = k_1 k_2 \dots k_L$, such that k_l corresponds to the l -th octal digit of K_i , counting from the most significant digit. The resulting ordering of internal octree nodes before the sorting step is equal to what one would get by first constructing a binary radix tree on top of K according to Karras, followed by enumeration and extraction of the octree nodes with a prefix sum. Indeed, we deduced Eq. (10)

Table 1: Timings for tree operations on an AMD EPYC 7713 64-core CPU, MI250X GPU and an NVIDIA A100 GPU. Either 1, 32 or 512 million particles were distributed with a 3D Gaussian density profile and N_{crit} was set to 64. The resulting octrees have 55.8K, 1.78M and 28.9M leaves, respectively. The radix sort step was implemented with `sort_by_key` from the Thrust library on both the CPU and GPU, with the particle SFC keys provided as keys and the identity permutation as values to keep track of the ordering.

<i>execution on CPU</i>	1M	32M	512M
64-bit Morton keys	2.2 ms	33 ms	520 ms
64-bit Hilbert keys	3.2 ms	107 ms	1640 ms
Radix sort	23 ms	607 ms	13100 ms
Leaf update (Sec. 4)	0.47 ms	32 ms	151 ms
Internal nodes (steps 1-5)	2.6 ms	80 ms	1400 ms
<i>execution on MI250X</i>	1M	32M	512M
64-bit Morton keys	0.041 ms	0.81 ms	13 ms
64-bit Hilbert keys	4.3 ms	7.3 ms	43 ms
Radix sort	0.925 ms	22 ms	330 ms
Leaf update (Sec. 4)	0.14 ms	0.81 ms	5.8 ms
Internal nodes (steps 1-5)	4.9 ms	6.3 ms	24 ms
<i>execution on A100</i>	1M	32M	512M
64-bit Morton keys	0.018 ms	0.31 ms	7.9 ms
64-bit Hilbert keys	0.084 ms	1.9 ms	30 ms
Radix sort	0.483 ms	5.0 ms	73 ms
Leaf update (Sec. 4)	0.11 ms	0.51 ms	2.5 ms
Internal nodes (steps 1-5)	0.19 ms	0.65 ms	5.4 ms

from the layout of the binary radix tree by induction under the assumption that each internal node has 8 children.

Additional octree node properties, such as particle counts, expansion centers, multipole moments, etc can be stored in separate arrays of length n and may be constructed in subsequent steps when required. We choose a breadth-first ordering of the octree nodes to ensure that the child nodes of each cell are always next to each other and to allow for efficient traversal in Barnes-Hut treecodes [3, 5].

Finally, to provide an overview of the relative costs of the steps involved in the tree construction, we list in Table 5 timings for 1, 32 and 512 million particles resulting in octrees with 55800, 1.78 million and 28.9 million leaf nodes, respectively.

6 DISTRIBUTED OCTREES AND DOMAIN DECOMPOSITION

In the case where particles and their sorted SFC keys \mathbf{P} are distributed across multiple compute nodes, we have to extend the algorithm in Sec. 4 with a communication scheme. With a small modification, we can identically replicate across compute nodes the octree that arises from the globally unified set of particles. To that end, after applying f , we perform an element-wise global sum of the histogram counts array \mathbf{N} :

$$f_{glob} = f_r \circ f, \quad (11)$$

where f_r simply computes an element-wise global sum of \mathbf{N} . The additional reduction step f_r can be implemented with a single call to `MPI_Allreduce`, supplying \mathbf{N} as argument. Initializing \mathbf{K} to the root node on all compute nodes, followed by an alternating application of f_{global} and g until converged, then yields the balanced cornerstone array, replicated on all compute nodes, for the distributed set of SFC keys \mathbf{P} . Due to the global collective communication pattern of f_r , this method is not suitable for generating octrees with a high resolution. However, it is fast enough for generating a global octree with sufficient resolution for decomposing the global domain by partitioning the space filling curve. The global domain can then be partitioned into n_{ranks} subdomains by grouping \mathbf{K} into n_{ranks} bins of consecutive leaves such that each bin contains approximately N_{tot}/n_{ranks} of the total particle count. Each bin covers a unique SFC key range that defines a compact volume of fractal-like shape. Our domain decomposition based on a coarse globally replicated octree requires collective communication that scales as $\mathcal{O}(N_{tot} \log N_{tot})$ and presents an alternative to other methods, such as sampling of the SFC [4, 7] which scales as $\mathcal{O}(N_{tot}^2)$ [22].

7 LOCALLY ESSENTIAL OCTREES

7.1 Definition

Let us assume that we have decomposed the global domain into n_{ranks} subdomains as described in Sec. 6. In order for the domain decomposition to balance the subdomain particle counts roughly within $p\%$ of N_{tot}/n_{ranks} -th where N_{tot} is the total global number of particles, only about $100/p$ leaf nodes are needed per subdomain. Consequently, the global tree will have a leaf node count resolution of $N_{crit} = \frac{N_{tot} \cdot p}{n_{ranks} \cdot 100}$ which is far too coarse for efficiently calculating physical forces for particles within a subdomain. What would be the requirements of a LET that facilitates the calculation of forces within just one subdomain, containing only the minimum number of nodes required for that task? In order to address this question, we need to introduce some physical context.

Two important types of forces covering a wide range of physical applications are

- Short-range forces with a cutoff. Examples: Smoothed Particle Hydrodynamics (SPH), Van-der-Waals dispersion in molecular dynamics
- Long-range forces arising from $1/r$ potentials. Examples: gravity and electrostatics

For the calculation of short-range forces, the octree has to have a high resolution (small N_{crit}) inside a given subdomain F for accurate neighbor particle searches. Additionally, a high resolution is also required close to the exterior surface for the discovery of halo particles.

Concerning long-range forces, we assume that the algorithm used to calculate them is either the Barnes-Hut treecode or FMM. Inside and close to the exterior surface of F , the tree resolution requirements are identical to the short-range case. Outside F however, a geometrical criterion, commonly called Multipole Acceptance Criterion (MAC), applies. For a given source tree node and target point or node, the MAC describes whether the application of the multipole approximation of the force due to the source on the target is acceptable or not. What all MACs have in common is that the

largest acceptable size of a source node correlates with the opening angle, i.e. the ratio between source node size and distance to the target. One of the simplest possible MAC choice is the minimum distance MAC, which is fulfilled if

$$r_{\min} > l/\theta, \quad (12)$$

where r_{\min} is the minimum distance between source and target, l is the source node edge length and θ is an accuracy parameter. The smaller the value for θ becomes, the smaller the error of the resulting force. More sophisticated acceptance criteria that depend on additional node properties exist and are compatible with our definition of an LET that follows.

Let F be a subdomain covering a contiguous range of the space filling curve. An octree, represented by the cornerstone array \mathbf{K}^{foc} , is locally essential in F or focused on F if

- (1) Leaves in F have a particle count $\leq N_{\text{crit}}$ while the counts of internal nodes in F exceed N_{crit} , i.e. they are balanced per the definition in Sec. 4.
- (2) Leaves outside F either pass the chosen MAC with respect to any point in F or their particle count is smaller than N_{crit} . The motivation for this condition is to make sure that when Barnes-Hut treecode or FMM is applied to particles in F , if tree traversal encounters a leaf node outside F , either the multipole approximation is valid or it contains only a small number of particles that can be transferred at a small cost. Consequently, refinement of nodes at the exterior surface of F stops once particle counts drop below N_{crit} as illustrated in Fig. 4.
- (3) Internal nodes outside F fail the chosen MAC for at least one point or node in F and their particle count is $> N_{\text{crit}}$. This ensures that the local tree depth is the minimum required to satisfy condition 2.

If we assume that particles within F reside on a particular compute node that additionally holds a copy of the halo particles close to the surface, the definition of the LET ensures that we will be able to compute long-range forces for particles in F depending on global information without the need for access to particle data beyond F and its surface. Insofar, it is important to note that the LET still covers the entire global domain.

7.2 Construction

As was the case for local or globally replicated octrees, we represent a LET with a cornerstone array. The general iterative construction scheme that yields an octree that satisfies the LET definition also remains largely the same: for each leaf node, the decision to either subdivide, keep, or merge it is encoded in the same fashion, i.e. functions g_2 and g_3 apply without modification. What is different is that apart from the node counts array \mathbf{N}^{foc} , the rebalancing operations to be performed now depend on a second array \mathbf{M} containing MAC evaluations and that the determination of \mathbf{N}^{foc} requires a combination of collective and point-to-point communication. The MAC evaluations stored in array \mathbf{M} are performed by a function denoted f_2^{LE} which traverses the octree defined by \mathbf{K}^{foc} . The result of f_2^{LE} are boolean values for each octree node outside F that describes whether there exists a leaf in F combined with which the MAC fails. If one chooses the minimum distance MAC, the evaluation

only depends on the geometrical size and location of the tree nodes and thus does not require communication. More adaptive MAC variants may rely on additional tree node properties, however, such as multipole expansion centers, which have to be computed prior to evaluating the MACs and will require communication. As the computation of \mathbf{M} involves tree traversal, f_2^{LE} constructs the fully linked octree that matches the leaf nodes \mathbf{K}^{foc} according to the procedure described in Sec. 5.

An update cycle that refines the LET from \mathbf{K}^{foc} to \mathbf{K}'^{foc} consists of the following steps:

$$f_1^{\text{LE}} : (\mathbf{P}, \mathbf{K}^{\text{foc}}, \mathbf{K}^{\text{glob}}, \mathbf{N}^{\text{glob}}) \mapsto \mathbf{N} \quad (\text{particle counts}) \quad (13)$$

$$f_2^{\text{LE}} : \mathbf{K}^{\text{foc}} \mapsto \mathbf{M} \quad (\text{MAC evaluations}) \quad (14)$$

$$g^{\text{LE}} : (\mathbf{K}^{\text{foc}}, \mathbf{N}^{\text{foc}}, \mathbf{M}) \mapsto \mathbf{K}'^{\text{foc}}, \quad (\text{rebalancing}) \quad (15)$$

where \mathbf{K}^{glob} is the cornerstone array of the globally replicated octree used for domain decomposition. We again distinguish between functions labelled f which compute node properties without modifying the octree, such as \mathbf{N} and \mathbf{M} , and functions labelled g which rebalance the octree based on said properties. A further distinction between the two groups is that the computation of node properties requires communication, while rebalancing consists of local operations only. The function g^{LE} decomposes into steps $g^{\text{LE}} = g_1^{\text{LE}} \circ g_2 \circ g_3$ with

$$g_1^{\text{LE}} : (\mathbf{K}^{\text{foc}}, \mathbf{N}^{\text{foc}}, \mathbf{M}) \mapsto \mathbf{O}, \quad (\text{rebalancing decision}) \quad (16)$$

and g_2 and g_3 as defined in Sec. 4. For nodes inside F , g_1^{LE} is identical to g_1 , i.e. only particle counts are taken into account to compute the corresponding elements of \mathbf{O} . Outside F , the result of g_1^{LE} depends on the particle counts as well as the MAC evaluations: a node is only split if the particle count exceeds N_{crit} and also the MAC evaluation failed. Conversely, a node is merged if its parent node either has a particle count smaller than N_{crit} or if the parent passed the MAC evaluation.

The most demanding function to implement is f_1^{LE} . It calculates node properties of the LET which can be computed by an upward pass. This applies to properties where the leaves depend on the contained particles and internal nodes on their children. Examples are given by node particle counts \mathbf{N} , multipole expansion centers, i.e. center-of-mass for gravity, and multipole moments. In the following, we assume that the domain decomposition was carried out based on \mathbf{K}^{glob} , assigning to each MPI rank a subdomain F along with the particles contained therein. The aim of f_1^{LE} is now to compute an array \mathbf{Q} of node properties arranged in the same layout as the nodes of the fully linked octree that can be constructed on top of \mathbf{K}^{foc} . Our strategy is to first construct the elements of \mathbf{Q} that correspond to the leaf nodes as this allows each rank to obtain the internal part through an upward pass without any further communication. The elements of \mathbf{Q} that correspond to leaves in \mathbf{K}^{foc} fall into three different categories which are illustrated in Fig. 3:

- (1) inside F between keys k_2 and k_3
- (2) outside F and exceeding the resolution of the global octree between keys k_1 to k_2 and k_3 to k_4 .
- (3) outside F and contained in \mathbf{K}^{glob} to the left of k_1 and to the right of k_4 .

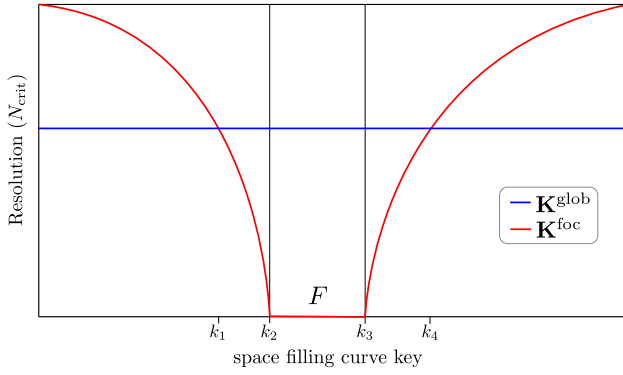


Figure 3: Resolution in terms of N_{crit} of the global octree and LET along the space filling curve. The line for K^{foc} outside F is drawn schematically. If plotted true to scale, K^{foc} would fall below K^{glob} in several areas, not just to the left and right of F . Note that the straight line for the global octree does not imply a regular grid structure; octree nodes of varying sizes manifest in this plot as stretches of different lengths along the x -axis.

While properties of leaves inside F can be directly computed based on local particle data, the second category involves point-to-point communication with nearby subdomains, and the third category involves collective communication followed by an upward pass of the global octree. Before any communication can take place, each rank must first build the fully linked octree on top of K^{foc} , compute the elements of \mathbf{Q} tied to leaves in F and perform an upward pass. This yields a partially filled property array \mathbf{Q} containing valid data for any node contained in F . Additionally, each rank determines a list of peer ranks that contain category 2 tree nodes in their subdomains by traversing the global octree. Point-to-point communication and collective communication may then proceed in parallel. The former is performed in two steps: in a first round of point-to-point messages, each rank sends a request to its peers that defines a series of octree nodes. As only leaf nodes are requested, the messages contain sub-sequences of K^{foc} . On the receiving side, the transmitted octree nodes may correspond to either leaf or internal nodes of the LET. An answer is then assembled by locating each requested octree node in the LET of the receiver and extracting the corresponding elements of \mathbf{Q} . The point-to-point exchange concludes with a second round of messages where the peer ranks send the required properties back to the requester. In order to obtain the remaining properties of nodes that fall into the third category, we construct an auxiliary array of properties \mathbf{Q}^{glob} whose node layout matches the fully linked octree constructed from K^{glob} . Each rank has the required data to populate the leaf nodes of \mathbf{Q}^{glob} that fall into its subdomain. We can then perform an *MPI_Allgather* operation on the \mathbf{Q}^{glob} array to replicate the leaf node quantities on all ranks. A subsequent upward pass of \mathbf{Q}^{glob} yields the internal nodes up to the global root node. Finally, each rank can complete the leaves of \mathbf{Q} by extracting the missing nodes from \mathbf{Q}^{glob} . Since some internal nodes in the LET may exist outside F and also not appear in the global octree, a second upsweep of \mathbf{Q} is needed to

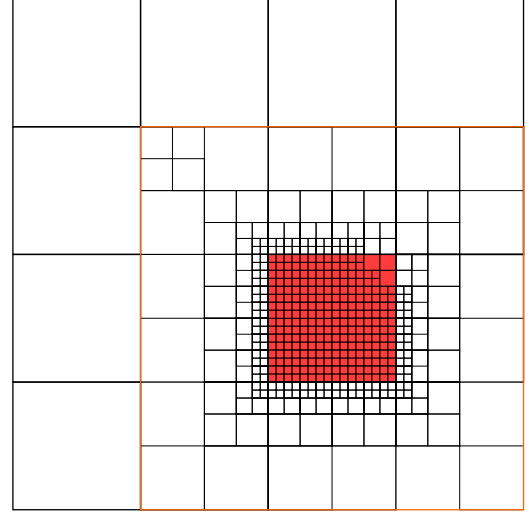


Figure 4: Example of a locally essential quadtree with the focus area F highlighted in red. The orange frame encompasses the part of K^{foc} where the resolution exceeds K^{glob} .

complete its construction. The final properties may then serve as the basis for particle force computations and as criteria to rebalance K^{foc} in Eq. (15).

We implement all stages of LET generation on GPUs. In addition to the operations discussed in Sec. 4, this involves an upsweep in f_2^{LE} and evaluating MACs in f_2^{LE} , for which we employ fully linked octrees constructed on top of K^{glob} and K^{foc} . After the application of Eqs. (13) to (15) no longer result in any changes to the LET, an analogous locally essential quadtree might look as shown in Fig. 4. In general, the resolution will be highest in the focus area F highlighted in red and decrease when moving away from F . But since the local particle density is also taken into account, the tree structure does not necessarily follow a uniform geometrical pattern. In our construction scheme, both K^{glob} and K^{foc} are stored in cornerstone format which is also used exclusively as the format for communication. Fully linked octrees are constructed on-demand on top of K^{glob} and K^{foc} . They are not preserved between time-steps. The collective communication that we perform on \mathbf{Q}^{glob} scales as $O(n_{\text{ranks}} \log n_{\text{ranks}})$ if the number of particles per MPI rank is kept constant, which is worse than the theoretical optimum of $O(\log n_{\text{ranks}})$. Due to the dynamically changing fractal sub-domain geometries that result from dividing the SFC into segments, a strictly hierarchical $O(\log n_{\text{ranks}})$ communication scheme that does not resort to collective communication for the highest levels of the LET where nodes transcend the sub-domain boundaries is very difficult to implement. This fact was also pointed out in Ref. [4], and, to the best of our knowledge, remains an unsolved problem.

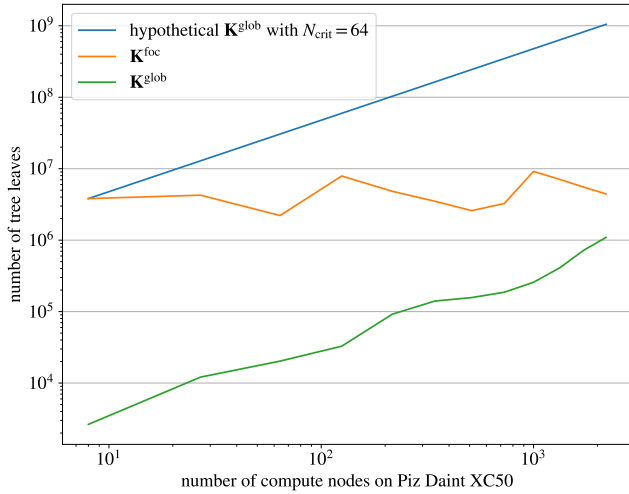


Figure 5: Scaling of the global octrees and LETs with system size between 64 million and 141 billion particles. The number of particles per compute node was kept constant at 64 million.

8 RESULTS

To assess the impact of the LET on the required size of the global octree, we create a spherical particle distribution with density inversely proportional to the radius and distribute it on varying numbers of compute nodes each running one MPI rank assigned with one subdomain constructed according to the method described in Sec. 6. The radius of the sphere is kept constant and each compute node holds a constant count of 64 million particles. With increasing number of compute nodes and total number of particles, the density of the sphere increases while the volumes of the subdomains decrease. For system sizes between 64 million and 141 billion particles, we construct LETs with $N_{crit} = 64$ and compare the resulting number of tree leaves against the leaf counts of K^{glob} (i.e. the global octree used for domain decomposition) and against a hypothetical octree with a uniform resolution of $N_{crit} = 64$ everywhere. In Fig. 5, we observe that LET growth is consistent with the expected $O(\log n_{ranks})$ behavior. By construction, K^{glob} grows linearly and will eventually exceed the size of K^{foc} , but it is roughly three orders of magnitude smaller compared to the octree with high uniform resolution that would be required in the absence of a LET.

In order to compare the cost of communication and computation, we implement a highly optimized version of Barnes-Hut treecode and compare the time required for the tree traversal with the time it takes to compute the multipole moments for the LET by applying f_1^{LE} . We used the treecode available at <https://github.com/exafmm/bonsai> as a starting point, a modified version of the original Bonsai code [5] with breadth-first traversal for GPUs. We further modified this code by changing the octree structure to our LET, replacing PTX inline assembly instructions from the NVIDIA Kepler microarchitecture with portable warp-level instructions for compatibility with AMD GPUs, and by adding

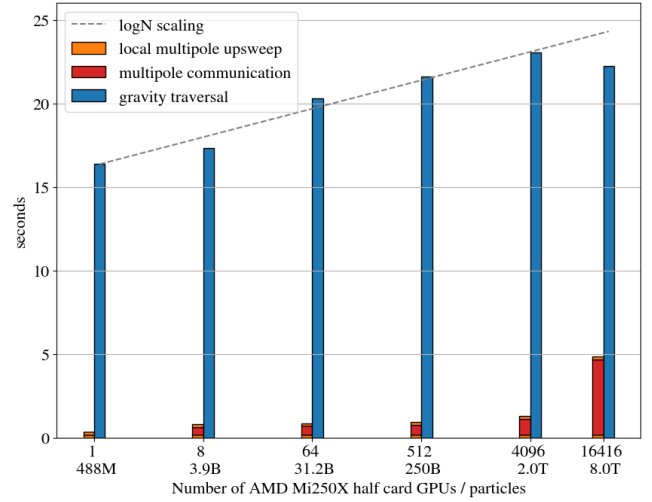


Figure 6: Barnes-Hut weak scaling on LUMI-G with 488 million particles per GPU and 8 trillion particles across 2052 computing nodes. The blue bars show the time required for traversing the LET to compute accelerations. Timings for multipole construction are subdivided into local compute and communication parts. Floating point operations were carried out in double precision.

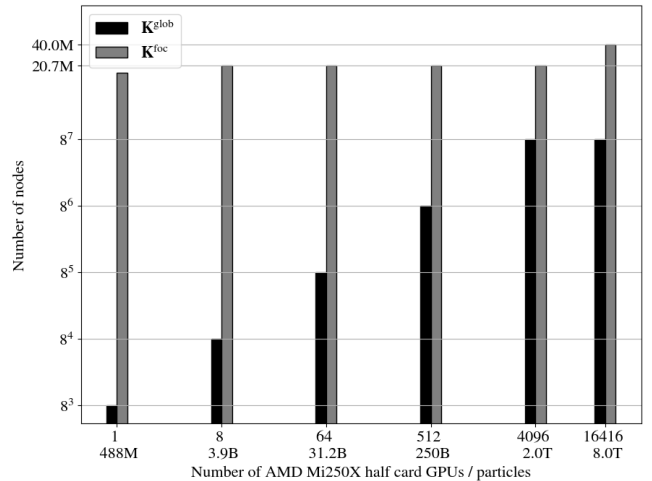


Figure 7: Scaling of LET and global octree node counts with system size.

further optimizations. In Fig. 6, we test the performance and scalability of our Barnes-Hut implementation on the LUMI-G system that features compute nodes with 4 AMD Instinct MI250X GPU cards. Each card contains two chips that appear as two separate GPUs and as a consequence, we ran our tests with 8 MPI ranks per compute node.

Our choice of cartesian multipoles with quadrupole corrections and $\theta = 0.5$ results in three significant digits in the computed particle accelerations. As described in Sec.7, the LET multipole

computation consists of two local upsweeps with a communication phase in between. After the first local upsweep is complete, it is possible to launch the tree traversal starting from the top LET nodes spanning the local sub-domain in order to achieve overlap with the multipole communication phase. Once the traversal of the local nodes completes, the remaining LET parts can be traversed by providing the LET nodes to the left and right of the local sub-domain on the SFC as starting points. For obtaining the results shown in Fig. 6, we did not overlap multipole construction with tree traversal and instead imposed a synchronization barrier in between to properly separate the timings for the two operations recorded as maxima across ranks. To estimate achieved performance in terms of Flops, we collected interaction statistics on one rank, counting the average number of particle-particle (P2P) and multipole-particle (M2P) interactions accrued during traversal per particle. In accordance with Ref. [4], counting P2P and M2P interactions as 23 and 65 flops, respectively, we estimate the performance per rank and MI250X half card at 6.7 Tflops in double precision, reaching a peak performance of 110 Pflops for the largest run with 8 trillion particles on 2052 nodes or 16416 GPU half cards, the maximum we were able to use. Note that the jump in communication time for the exchange of multipole moments when moving from 2 to 8 trillion particles is not due to an increase in collective communication. As shown in Fig. 7, the number of nodes in the global octree is in fact identical between the last two data points. The difference in communication time is caused by the larger number of LET nodes in the largest run. This is simply a consequence of the average number of particles per leaf node in the LET fluctuating between $\approx N_{\text{crit}}/8$ and N_{crit} (64), explaining the shorter traversal time on 16416 GPUs as well. While the average number of particles per leaf was around 30 on 1 to 4096 GPUs, the average dropped to 12 for the system with 8 trillion particles, resulting in higher traversal efficiency by reducing the number of P2P interactions per particle.

9 SUMMARY AND FUTURE WORK

We have shown that octrees can be efficiently constructed on GPUs with the presented algorithms. The resulting octrees and LETs are suited to supporting the computation of short and long-ranged forces acting on particles and can be constructed at scale on distributed HPC systems. Relative to a competitive Barnes-Hut treecode implementation, LET construction overhead remains small enough to allow for nearly complete overlap with the tree traversal phase on almost the full LUMI-G HPC system. Our future goal is to employ Cornerstone for an interesting scientific application, for example by combining our N-body solver with SPH.

9.1 Software availability

The algorithms described in this work have been implemented in C++, CUDA and HIP, and are available as open-source software. Octrees, LETs, neighbor searching and domain decomposition are bundled into the Cornerstone library available at <https://github.com/sekelle/cornerstone-octree>. It does not implement any physics, such as Barnes-Hut or FMM for gravity. Cornerstone is integrated into a full-fledged application framework called SPH-EXA, available at <https://github.com/unibas-dmi-hpc/SPH-EXA>. SPH-EXA can perform I/O, generate initial conditions and offers

SPH and gravity (described in Sec. 8) as composable components for physical simulations. Efforts are underway to also make our Barnes-Hut implementation available as a stand-alone package.

ACKNOWLEDGMENTS

This work was supported by the Swiss Platform for Advanced Scientific Computing (PASC) project SPH-EXA (funding periods 2017-2021 and 2021-2024). We acknowledge the support of the LUMI-G pilot program hosted by CSC, in particular Emmanuel Ory, Pekka Manninen and Fredrik Robertsén, and the Swiss National Supercomputing Center (CSCS) for providing access to the Piz Daint supercomputer.

REFERENCES

- [1] C Apetrei. 2014. Fast and Simple Agglomerative LBVH Construction. In *Computer Graphics and Visual Computing (CGVC)*. The Eurographics Association. <https://doi.org/10.2312/cgvc.20141206>
- [2] J Barnes and P Hut. 1986. A hierarchical O (N log N) force-calculation algorithm. *Nature* 324, 6096 (1986), 446–449.
- [3] Joshua E Barnes. 1990. A modified tree code: Don't laugh; it runs. *J. Comput. Phys.* 87, 1 (1990), 161–170.
- [4] Jeroen Bedorf, Evghenii Gaburov, Michiko S. Fujii, Keigo Nitadori, Tomoaki Ishiyama, and Simon Portegies Zwart. 2014. 24.77 Pflops on a Gravitational Tree-Code to Simulate the Milky Way Galaxy with 18600 GPUs. In *SC14: International conference for high performance computing, networking, storage and analysis*. 54–65. <https://doi.org/10.1109/SC.2014.10> International Conference on High Performance Computing, Networking, Storage and Analysis, New Orleans, LA, Nov 16-21, 2014.
- [5] Jeroen Bedorf, Evghenii Gaburov, and Simon Portegies Zwart. 2012. A sparse octree gravitational N-body code that runs entirely on the GPU processor. *J. Comput. Phys.* 231, 7 (Apr 1 2012), 2825–2839. <https://doi.org/10.1016/j.jcp.2011.12.024>
- [6] N Bell and J Hoberock. 2022. Thrust 1.17. <https://github.com/nvidia/thrust>.
- [7] D Blackston and T Suel. 1997. Highly portable and efficient implementations of parallel adaptive n-body methods. In *Proceedings of the 1997 ACM/IEEE Conference on Supercomputing*. 1–20.
- [8] Martin Burtscher and Keshav Pingali. 2011. An efficient CUDA implementation of the tree-based barnes hut n-body algorithm. In *GPU computing Gems Emerald edition*. Elsevier, 75–92.
- [9] RA Gingold and JJ Monaghan. 1977. Smoothed particle hydrodynamics: theory and application to non-spherical stars. *MNRAS* 181, 3 (1977), 375–389.
- [10] L Greengard and V Rokhlin. 1987. A fast algorithm for particle simulations. *J. Comput. Phys.* 73, 2 (1987), 325–348.
- [11] Herman Haverkort. 2011. An inventory of three-dimensional Hilbert space-filling curves. *arXiv preprint arXiv:1109.2323* (2011).
- [12] Lars Hernquist. 1987. Performance characteristics of tree codes. *The Astrophysical Journal Supplement Series* 64 (1987), 715–734.
- [13] David Hilbert. 1891. Ueber die stetige Abbildung einer Linie auf ein Flächenstück. *Math. Ann.* 38 (1891), 459–460.
- [14] T Karras. 2012. Maximizing parallelism in the construction of BVHs, octrees, and k-d trees. In *Proceedings of the Fourth ACM SIGGRAPH/Eurographics conference on High-Performance Graphics*. 33–37.
- [15] Steffen R Knollmann and Alexander Knebe. 2009. AHF: Amiga's halo finder. *The Astrophysical Journal Supplement Series* 182, 2 (2009), 608.
- [16] LB Lucy. 1977. A numerical approach to the testing of the fission hypothesis. *AJ* 82 (1977), 1013–1024.
- [17] Guy M Morton. 1966. A computer oriented geodetic data base and a new technique in file sequencing. (1966).
- [18] G Peano. 1890. Sur une courbe, qui remplit toute une aire plane. *Math. Ann.* 36 (1890), 157–160.
- [19] Albino Perego, Emanuel Gafton, Rubén Cabezón, Stephan Rosswog, and Matthias Liebendörfer. 2014. MODA: a new algorithm to compute optical depths in multi-dimensional hydrodynamic simulations. *aap* 568, Article A11 (Aug. 2014), A11 pages. <https://doi.org/10.1051/0004-6361/201423755> arXiv:1403.1297 [astro-ph.HE]
- [20] Douglas Potter, Joachim Stadel, and Romain Teyssier. 2017. PKDGRAV3: beyond trillion particle cosmological simulations for the next era of galaxy surveys. *Computational Astrophysics and Cosmology* 4, 1 (2017), 1–13.
- [21] DS Shamshirgar, R Yokota, AK Tornberg, and B Hess. 2019. Regularizing the fast multipole method for use in molecular simulation. *The Journal of Chemical Physics* 151, 23 (2019), 234113. <https://doi.org/10.1063/1.5122859> arXiv:https://doi.org/10.1063/1.5122859

- [22] Robert Speck, Lukas Arnold, and Paul Gibbon. 2011. Towards a petascale tree code: Scaling and efficiency of the PEPC library. *Journal of Computational Science* 2, 2 (2011), 138–143.
- [23] MS Warren and JK Salmon. 1993. A Parallel Hashed Oct-Tree N-Body Algorithm. In *Supercomputing '93, Proceedings (Supercomputing Proceedings)*. 12–21. Supercomputing 93 Conference, Portland, OR, Nov 15-19, 1993.
- [24] Michael S Warren and John K Salmon. 1992. Astrophysical N-body simulations using hierarchical tree data structures. *SC 92 (1992)*, 570–576.
- [25] Rio Yokota. 2013. An FMM based on dual tree traversal for many-core architectures. *Journal of Algorithms & Computational Technology* 7, 3 (2013), 301–324.

A TABLES OF SYMBOLS

Table 2: Symbols introduced in Sec. 4 involved in the construction of octree leaves.

<i>symbol</i>	<i>description</i>
L	maximum octree depth
\mathbf{K}	cornerstone leaf node SFC key array, Eq. (2)
n_l	number of leaf nodes in \mathbf{K}
\mathbf{N}	leaf node particle counts array
N_{crit}	maximum number of particles per leaf
\mathbf{P}	array of local particle SFC keys
f	leaf node particle counting function
$g, g_{1,2,3}$	functions to rebalance \mathbf{K}
\mathbf{O}	auxiliary array for node transformation operations

Table 3: Symbols introduced in Sec. 5 involved in the construction of fully linked octrees.

<i>symbol</i>	<i>description</i>
\mathbf{NK}	array of node keys for internal and leaf nodes
n_i	number of internal nodes
n	total number of nodes, $n = n_i + n_l$
\mathbf{CO}	child connectivity array
\mathbf{LO}	octree level offsets
δ	mapping between leaf and internal nodes
d	number of common leading bits of two SFC keys

Table 4: Symbols introduced in Sec. 6 involved in the construction of distributed and globally replicated octrees.

<i>symbol</i>	<i>description</i>
f_r	<i>MPI_Allreduce</i>
f_{glob}	combination of f with f_r
n_{ranks}	number of MPI ranks or subdomains
N_{tot}	total number of particles across all ranks

Table 5: Symbols introduced in Sec. 7 involved in the construction of focused octrees, also known as LETs.

<i>symbol</i>	<i>description</i>
F	a subdomain corresponding to a section of the SFC
\mathbf{K}^{foc}	cornerstone array of an octree focused on F
\mathbf{N}^{foc}	particle counts of nodes in \mathbf{K}^{foc}
\mathbf{K}^{glob}	cornerstone array of a globally replicated octree
\mathbf{N}^{glob}	particle counts of nodes in \mathbf{K}^{glob}
θ	angle-based accuracy parameter
\mathbf{M}	array of length n with MAC evaluation results
f_1^{LE}	particle counting function for nodes \mathbf{K}^{foc}
f_2^{LE}	MAC evaluation function
$g^{\text{LE}}, g_1^{\text{LE}}$	functions to rebalance \mathbf{K}^{foc}
\mathbf{Q}	generic node properties of a fully linked LET
\mathbf{Q}^{glob}	generic node properties of a globally replicated octree